



Synthesis, fluorescence properties and F⁻ detection performance of Eu (III) complexes based on the novel coumarin Schiff base derivatives

Fangfei Luan, Gangxiang Xiao, Yuxi Zhang, Shiquan Li, Zhongqian Hu, Hongli Du, Dongcai Guo*

State Key Laboratory of Chemo/Biosensing and Chemometrics, College of Chemistry and Chemical Engineering, Hunan University, Changsha 410082, China

ARTICLE INFO

Article history:

Received 12 August 2020

Received in revised form 12 September 2020

Accepted 23 September 2020

Available online 30 September 2020

Keywords:

AIE property

Eu(III) complex

Fluorescence property

Electro-chemical property

Ion detection

ABSTRACT

Three novel coumarin Schiff base derivatives and corresponding Eu(III) complexes were designed and synthesized. The aggregation-induced emission (AIE) property of ligands was studied. The fluorescence properties and electrochemical properties of Eu(III) complexes were investigated by comparing different substituent groups. The ion selectivity and ion detection limits of the [EuL²(NO₃)₃]•H₂O were also studied. The result indicates that all ligands exhibit the AIE property in CH₃CN/H₂O solution and emit green fluorescence with the maximum emission wavelength of 552 nm. All complexes show characteristic red fluorescence of Eu(III) and the influence of different substituents on the fluorescence intensity of Eu(III) complexes is ordered: -OCH₃ > -H > -NO₂, and [EuL²(NO₃)₃]•H₂O exhibits the strongest fluorescence intensity. The density functional theory (DFT) calculations of the ligands indicate that the introduction of electron-donating groups increases the HOMO energy level and the electron cloud density, which enhance the ability to coordinate with Eu(III) and the fluorescence intensity of the corresponding complex. Besides, the electrochemical properties of Eu(III) complexes indicate that the introduction of electron-donating groups increases the energy gaps (E_g) and the conjugation of the complex, which enhances the fluorescence intensity of the complexes. Ion selectivity experiments show that [EuL²(NO₃)₃]•H₂O has a specific recognition function for F⁻, and its response limit is between 1.0 × 10⁻⁵ mol·L⁻¹ and 2.2 × 10⁻⁵ mol·L⁻¹. Based on the above results, all the ligands and Eu(III) complexes have a promising application in optical materials due to the excellent fluorescence properties. In addition, All Eu(III) complexes also have a potential application prospects in the field of fluoride ion detection.

© 2020 Elsevier B.V. All rights reserved.

1. Introduction

In recent years, lanthanide complexes have been widely used in catalysis, sensors, magnetic recording materials and optical materials fields based on their special porous cavities and notable electronic features [1–5]. Among many rare earth complexes, Eu(III) complexes have pure red fluorescence, long lifetime and good monochromaticity. These features enable a wide range of applications as optical probes for bioimaging and sensors. However, there are still some shortcomings that need to be overcome. For example, poor thermal stability, low luminous intensity and low electron transfer efficiency. The fluorescence intensity of lanthanide complexes mainly depends on two key factors: (1) Transfer efficiency of triplet energy level and luminescence level of ligands (2) The extent of non-radiative decay of excited state of lanthanide complexes [6]. Therefore, designing and synthesizing excellent fluorescent ligands is the key of this work.

In 2001, the phenomenon of aggregation-induced emission (AIE) was first reported by Tang and co-workers, which was explained by

the mechanism of restricted intramolecular rotations (RIR) [7,8]. Then, a lot of works have been done around the AIE effects, such as ion probes, biotherapeutics, optical materials, OLEDs and cancer detection, and so on [9–11]. Most of AIE materials have a large conjugated structure, which is a good choice as a luminescent ligand. Among many AIE materials, some Schiff-base materials with intramolecular proton transfer (ESIPT) properties have also been reported recently [12–14]. For the Schiff-base materials, most of them are used in organic catalysis synthesis, complexes and liquid crystal materials fields. Especially, in complexes fields, the Schiff-base derivatives often are selected as the ligand due to their ease of preparation and good coordination ability [15,16]. Therefore, designing and synthesizing Schiff-base derivatives with AIE properties is a good choice.

As we all know, coumarin derivatives are often used in the field of drug therapy and bioprobes, especially in the field of fluorescent materials [17–19]. Whether natural or artificial, the preparation of coumarin derivatives is relatively easy to obtain and low in cost. Besides, most hydroxy-coumarin compounds have a certain fluorescent property, which is also widely used in the field of fluorescent materials. In our previous works, some excellent ligands and complexes are synthesized, such as Schiff bases, pyrazolones, quinolines, and so on [20–23]. Most

* Corresponding author.

E-mail address: dccguo2001@hnu.edu.cn (D. Guo).

researchers focus on the function of complexes, and the complexes of AIE coumarin derivatives ligands has rarely been reported. Therefore, coumarin derivatives are also a good choice as ligands.

In this work, three novel coumarin Schiff base derivatives and corresponding Eu(III) complexes are synthesized and characterized by ^1H NMR, ^{13}C NMR, ESI-MS, UV-Vis, Molar conductivity, Elemental analysis, Thermogravimetric analysis and FT-IR analysis. The AIE property of the ligands is explored, and the influence of different substituents on the fluorescence and electrochemical properties of Eu(III) complexes is discussed. Besides, this work has further studied the ion detection performance of the complex with the best fluorescence performance. Correspondingly, the synthetic route of ligands (L^{1-3}) is presented in Scheme 1.

2. Experimental

2.1. Materials and physical measurements

The purity of Eu_2O_3 exceeded 99.99%, all reagents used were of AR grade without further purification.

^1H NMR and ^{13}C NMR were measured with a Bruker-400 MHz nuclear magnetic resonance spectrometer with deuterated chloroform (CDCl_3) or dimethyl sulfoxide ($\text{DMSO}-d_6$) as a solvent and TMS as internal reference. The electron impact mass spectra (ESI-MS) were measured using a MAT95XP analyzer. The UV-Vis spectra were recorded on a LabTech UV-2100 UV Spectrophotometer and dimethyl sulfoxide (DMSO) was used as a reference and a solvent. The FT-IR (KBr pellets) were recorded in the region $4000\text{--}400\text{ cm}^{-1}$ on a Shimadzu IRAffinity-1 FT-IR spectrophotometer. Elemental analysis was determined by Flash EA 1112 Elemental Analyzer. Thermal gravimetric (TG) were carried out up to $800\text{ }^\circ\text{C}$ with a heating speed of $10\text{ }^\circ\text{C}/\text{min}$ in the air atmosphere on an SHIM ADZU DTG-60 thermogravimetric analyzer. Fluorescence spectra were monitored by HIACHI F-2700 spectrophotometer at room temperature, the widths of both the excitation and emission slit were 5.0 nm and the voltage of photomultiplier tube was 700 V . Density functional theory (DFT) calculations were performed with Gaussian 09 program. Cyclic voltammetry (CV) measurements were performed

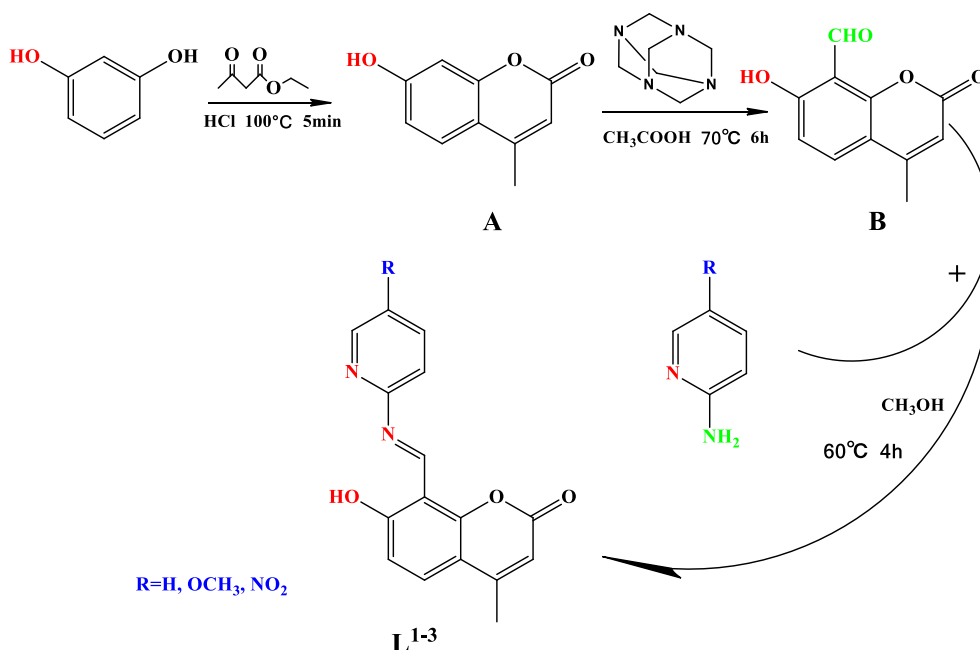
using a CHI 660d electrochemical workstation (electrolyte: 0.1 M tetrabutylammonium hexafluorophosphate, solvent: DMF, sensitivity: 0.1 mA/V , scan speed: 50 mV s^{-1}).

2.2. Synthesis methods

2.2.1. Synthesis of intermediates

2.2.1.1. 7-Hydroxy-4-methyl-2H-chromen-2-one (A). Resorcinol (2.20 g, 20 mmol), ethyl 3-oxobutanoate (1.30 g, 10 mmol) and concentrated HCl (5 mmol) were added to three-necked flask. The reaction was carried out at $100\text{ }^\circ\text{C}$ for 5 min in a microwave irradiation reaction, and TLC was monitored until the consumption of the reactants was completed. The reaction was then cooled to room temperature and an appropriate amount of cold water was added and a large white solid precipitated and then filtered. The precipitate was washed three times with cold water and dried in a vacuum oven. Off-white, yield: 87%, ^1H NMR (400 MHz, DMSO) δ ppm = 10.52 (s, 1H, OH), 7.61 (d, $J = 8.7\text{ Hz}$, 1H, ArH), 6.82 (dd, $J = 8.7, 2.3\text{ Hz}$, 1H, ArH), 6.72 (d, $J = 2.2\text{ Hz}$, 1H, ArH), 6.15 (s, 1H, ArH), 2.39 (s, 3H, CH_3). ^{13}C NMR (126 MHz, CDCl_3) δ 161.60 (s), 160.74 (s), 155.28 (s), 153.92 (s), 126.98 (s), 113.28 (s), 112.45 (s), 110.69 (s), 102.62 (s), 18.53 (s). ESI-MS (CH_2Cl_2) m/z : 175.12 ($\text{M} - 1$).

2.2.1.2. 7-Hydroxy-4-methyl-2-oxo-2H-chromene-8-carbaldehyde (B). 7-hydroxy-4-methyl-2H-chromen-2-one (1.76 g, 10 mmol), and hexamethylenetetramine (1.40 g, 10 mmol) were added to the round bottom flask with 15 mL acetic acid. Refluxing at $70\text{ }^\circ\text{C}$ for 6 h, 5 mL of water and 2 mL of concentrated hydrochloric acid were added after the reaction was cooled. The product was extracted with diethyl ether and recrystallized three times with ethanol to dryness. Light yellow solid, yield: 57%. ^1H NMR (400 MHz, CDCl_3) δ ppm = 12.27 (s, 1H, OH), 10.68 (s, 1H, C-H), 7.79 (d, $J = 9.0\text{ Hz}$, 1H, ArH), 6.97 (d, $J = 9.0\text{ Hz}$, 1H, ArH), 6.27 (s, 1H, ArH), 2.49 (s, 3H, CH_3). ^{13}C NMR (126 MHz, CDCl_3) δ 191.77 (s), 164.15 (s), 159.29 (s), 155.58 (s), 154.58 (s), 133.78 (s), 114.03 (s), 112.21 (s), 111.57 (s), 109.45 (s), 18.82 (s). ESI-MS (CH_2Cl_2) m/z : 203.00 ($\text{M} - 1$).



Scheme 1. Synthetic route of L^{1-3} .

2.2.2. Synthesis of L^{1-3}

2.2.2.1. (*E*)-7-hydroxy-4-methyl-8-((pyridin-2-ylimino)methyl)-2H-chromen-2-one L^1 . 7-HYDROXY-4-methyl-2-oxo-2H-chromene-8-carbaldehyde (0.20 g, 1 mmol) and pyridin-2-amine (0.01 g, 1 mmol) were added to the round bottom flask with 10 mL methanol. Refluxing at 60 °C for 4 h, the reaction was cooled to room temperature and a large orange precipitate was precipitated. Precipitate was washed three times with ethanol to give the final pure product. Light yellow solid, yield: 76%. $^1\text{H NMR}$ (400 MHz, CDCl_3) δ ppm = 15.33 (s, 1H, OH), 10.16 (s, 1H, C—H), 8.60 (d, $J = 4.5$ Hz, 1H, ArH), 7.85 (t, $J = 7.7$ Hz 1H, ArH), 7.65 (d, $J = 9.0$ Hz, 1H, ArH), 7.37 (d, $J = 7.9$ Hz 1H, ArH), 7.34–7.29 (m, 1H, ArH), 6.95 (d, $J = 9.0$ Hz, 1H, ArH), 6.19 (s, 1H, ArH), 2.47 (s, 3H, CH_3). $^{13}\text{C NMR}$ (126 MHz, CDCl_3) δ 168.63(s), 160.17(s), 158.35(s), 155.39(s), 153.11(s), 149.31(s), 138.55(s), 130.22(s), 122.98(s), 119.09 (s), 115.58(s), 110.95(s), 110.73(s), 106.82(s), 18.94(s). ESI-MS (CH_2Cl_2) m/z : 281.31 (M + 1).

2.2.2.2. (*E*)-7-hydroxy-8-((5-methoxy-pyridin-2-yl)imino)methyl)-4-methyl-2H-chromen-2-one L^2 . 7-Hydroxy-4-methyl-2-oxo-2H-chromene-8-carbaldehyde (0.20 g, 1 mmol) and 5-methoxypyridin-2-amine (0.12 g, 1 mmol) were added to the round bottom flask with 10 mL methanol. Refluxing at 60 °C for 4 h, the reaction was cooled to room temperature and a large orange precipitate was precipitated. Precipitate was washed three times with ethanol to give the final pure product. Light yellow solid, yield: 81%. $^1\text{H NMR}$ (400 MHz, DMSO) δ ppm = 15.39 (s, 1H, OH), 10.04 (s, 1H, C—H), 8.24 (s, 1H, ArH), 7.60 (d, $J = 9.0$ Hz, 1H, ArH), 7.31 (t, $J = 2.9$ Hz, 2H, ArH), 6.92 (d, $J = 9.0$ Hz, 1H, ArH), 6.16 (s, 1H, ArH), 3.95 (s, 3H, CH_3), 2.44 (s, 3H, CH_3). $^{13}\text{C NMR}$ (126 MHz, CDCl_3) δ 191.85(s), 164.18(s), 163.72(s), 155.66 (s), 154.15(s), 147.48(s), 134.84(s), 133.83(s), 133.09(s), 111.60(s), 109.56(s), 107.64(s), 56.49(s), 19.03(s). ESI-MS (CH_2Cl_2) m/z : 311.09 (M + 1).

2.2.2.3. (*E*)-7-hydroxy-4-methyl-8-((5-nitropyridin-2-yl)imino)methyl)-2H-chromen-2-one L^3 . 7-Hydroxy-4-methyl-2-oxo-2H-chromene-8-carbaldehyde (0.20 g, 1 mmol) and 5-nitropyridin-2-amine (0.14 g, 1 mmol) were added to the round bottom flask with 10 mL methanol. Refluxing at 60 °C for 4 h, the reaction was cooled to room temperature and a large orange precipitate was precipitated. Precipitate was washed three times with ethanol to give the final pure product. Red solid, yield: 76%. $^1\text{H NMR}$ (400 MHz, DMSO) δ ppm = 11.91 (s, 1H, OH), 10.47 (s, 1H, C—H), 8.79–8.64 (m, 1H, ArH), 7.96 (d, $J = 8.8$ Hz, 1H, ArH), 7.88 (d, $J = 8.5$ Hz, 1H, ArH), 7.63 (d, $J = 8.5$ Hz 1H, ArH), 6.81 (d, $J = 9.2$ Hz, 1H, ArH), 6.33 (s, 1H, ArH), 2.40 (s, 3H, CH_3). $^{13}\text{C NMR}$ (Poor sample solubility). ESI-MS (CH_2Cl_2) m/z : 325.16 (M + 1).

2.2.3. Synthesis of Eu(III) complexes

According to our previous reports [20], 0.20 mmol ligands were dissolved in 20 mL ethyl acetate at 60 °C, and 1 mL $\text{Eu}(\text{NO}_3)_3$ ethyl acetate solution was added. Then, pH was adjusted to 6–7 using 1 mol·L⁻¹ sodium ethoxide solution. After refluxing for 8 h, the mixture was cooled to room temperature and poured into petroleum ether, then washed with water (30 mL) and filtered to give a white solid. Finally, the Eu(III) complexes were obtained.

3. Results and discussion

3.1. The properties of ligands (L^{1-3})

This paper only studies the AIE properties of the ligands. The following is a detailed description of the AIE properties of the ligands. Since all ligand structures are similar, we choose the L^1 as an explanation. The AIE properties were measured in acetonitrile as a solvent (30 μM , pH = 7, 25 °C). The water fraction (fw) is the ratio of water to solvent (acetonitrile and water).

The fluorescence quantum yields of L^{1-3} in acetonitrile solvent were calculated based on the following formula by quinine sulfate as standard [24].

$$\Phi_{\text{fx}} = \frac{n_{\text{x}}^2}{n_{\text{std}}^2} \cdot \frac{F_{\text{x}}}{F_{\text{std}}} \cdot \frac{A_{\text{std}}}{A_{\text{x}}} \cdot \Phi_{\text{fstd}}$$

where std. and x represent the standard and the analyte, respectively, and n represents the refractive index of the solution ($n_{\text{x}(\text{C}_2\text{H}_3\text{N})} = 1.344$, $n_{\text{std}} = 1.337$). F represents the fluorescence integrated area, and A represents the ultraviolet absorbance. Φ_{fstd} represents the fluorescence quantum yield of the standard substance solution ($\Phi_{\text{fstd}} = 0.55$).

According to many related works reports, similar structures show excellent AIE properties. As expected, from the Fig. 1 and Table 1, the fluorescence intensity and fluorescence quantum yields of L^1 are significantly enhanced through the fw increases, and the green emission is exhibited. For the ligand, a typical intramolecular proton transfer phenomenon has been found in which a phenolic hydroxyl group interacts with C=N to fluoresce by interconversion between an enol isomer and a keto isomer [25–27]. When the ligand is dissolved in the solution, since the C=N pole is easily rotated, the conjugation of the molecule is affected, and the intramolecular proton transfer efficiency is lowered. Unlike the ACQ phenomenon (aggregation-caused quenching), the rotation of C=N is limited with the increase of fw, and the conjugation of molecules increases. The fluorescence intensity at fw = 0 is the weakest, and the fluorescence intensity is continuously enhanced by the increase of fw. Besides, the corresponding fluorescence quantum yields (Φ_{fx}) increase from 0.081 to 0.255, which also indicates that the ligand possesses AIE properties.

3.2. Characterization of the Eu(III) complexes

3.2.1. FT-IR spectral analysis and molar conductivity

In order to prove the structural information of the complexes, FT-IR and the molar conductivity were measured. All the complexes were soluble in DMSO, DMF, slightly soluble in ethanol, methanol, ethyl acetate and dichloromethane, insoluble in water, petroleum ether. Molar conductivity was measured in DMF (10⁻³ mol·L⁻¹, pH = 7, temperature = 25 °C), and the data was presented in Table S1 and Fig. 2 (Table S1 and FT-IR of L^2 , L^3 and $[\text{EuL}^2 \cdot 3(\text{NO}_3)_3] \cdot \text{H}_2\text{O}$ are provided in the support information). Since the structure is similar, we only choose L^1 and $[\text{EuL}^1(\text{NO}_3)_3] \cdot \text{H}_2\text{O}$ as an explanation [28,29].

As shown in Fig. 2 and Table S1, compared with the L^1 , the FT-IR of $[\text{EuL}^1(\text{NO}_3)_3] \cdot \text{H}_2\text{O}$ has undergone a very dramatic change, which indicates the Eu(III) complexes have been prepared successfully. For the L^1 , a certain intensity band at 3469 cm⁻¹ is found, which is assigned to the stretching frequency of the OH group. In addition, a high intensity band is observed at 1723 cm⁻¹, which is attributed to the typical stretching vibration of the C=O group [30]. Meanwhile, medium intensity bands are detected at 1691 cm⁻¹ and 1652 cm⁻¹ due to the different azomethine moieties, which is the C=N group of Schiff-base and pyridine ring, respectively [31]. For the Eu(III) complex, a broad high intensity band of the OH group is observed at 3451 cm⁻¹ with 18 cm⁻¹ red-shifts, which indicates the oxygen atom of the OH group coordinates to Eu(III) ions without deprotonating [32]. In addition, two $\nu_{\text{C=N}}$ are red shifted to 1667 cm⁻¹ and 1598 cm⁻¹ with 24 cm⁻¹ and 54 cm⁻¹ shifts, respectively, which are corresponding the characteristic band of the C=N group in Schiff-base and pyridine ring. The obvious shifts indicate that two C=N groups in Schiff-base and pyridine ring have been coordinated to Eu(III) ions through the nitrogen atom. However, we can notice that there is no significant shifts in the position of C=O group, which indicates that C=O group does not participate in the coordination. The characteristic peak of the ligand L^1 and the complex $[\text{EuL}^1(\text{NO}_3)_3] \cdot \text{H}_2\text{O}$ at 2920 cm⁻¹ correspond to the stretching vibration of saturated C—H [33], and the saturated C—H has no possibility of coordination with Eu^{3+} , we not discuss it too much here.

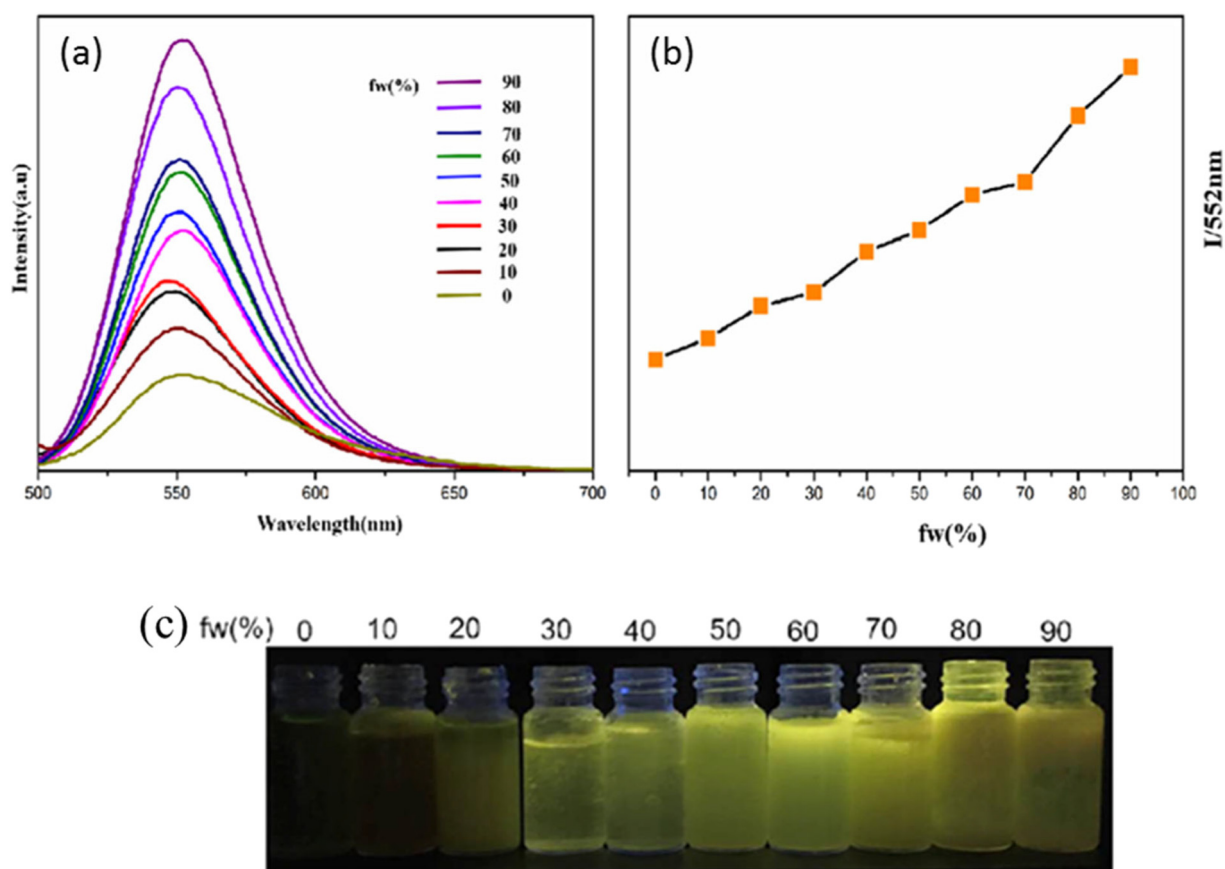


Fig. 1. (a) Fluorescence spectra under different fw (0%–90%) (b) Fluorescence intensity under different fw (0%–90%) (c) Fluorescence under different fw (0%–90%).

Different functional groups exhibit varying degrees of red shifts due to the conjugation of the molecules increases after coordination, the vibration frequency becomes lower, the wave number becomes lower, and the corresponding wavelength red shifts. Thus, we can infer that the OH group and two C=N groups are successfully coordinated with Eu(III) ions [34,35].

Meanwhile, the measured values of the molar conductivity are in the range of 23 to 27 $\text{Scm}^2\text{mol}^{-1}$, which indicates that the above materials are nonelectrolytes [36]. In other words, there is no free nitrate in the complex molecule. The characteristic frequencies of the coordinating nitrate groups appear at about 1370 cm^{-1} (ν_{as}), 1190 cm^{-1} (ν_2), 1020 cm^{-1} (ν_4) and 829 cm^{-1} (ν_s). The difference between the two highest frequency band ($\Delta\nu = \nu_{\text{as}} - \nu_2$) gives the information on the coordination of nitrate ions with rare earth ions [37,38]. From FT-IR data, the $\Delta\nu$ values of Eu(III) complexes are about 180 cm^{-1} , indicating three nitrate ions are coordinated with the Eu(III) ion in a bidentate fashion.

Therefore, we can deduce the ligands are coordinated with Eu(III) ion successfully. The functional group specifically involved in the coordination was determined, and the three nitrate groups successfully participated in the complexation in a bidentate fashion.

3.2.2. Elemental analysis, ESI-MS and TG analysis

To confirm the composition of Eu(III) complexes further, elemental analysis, ESI-MS and TG analysis of the complex were determined.

Table 1

Fluorescence quantum yields of L¹ in different fw (0%–90%).

f _w	0%	10%	20%	30%	40%	50%	60%	70%	80%	90%
Φ_{fx}	0.081	0.102	0.114	0.119	0.141	0.162	0.189	0.192	0.231	0.255

The data of elemental analysis of $[\text{EuL}^{1-3}(\text{NO}_3)_3] \cdot \text{H}_2\text{O}$ are listed in Table 2. We can see that the experimental data of the content C (29.96%), H(2.33%), N(11.86%), O(31.02%) and Eu(28.92%) in the $[\text{EuL}^1(\text{NO}_3)_3] \cdot \text{H}_2\text{O}$ are well consistent with the theoretical calculation values of C(30.18%), H(2.20%), N(11.00%), O(30.18%) and Eu(28.88%) in the $[\text{EuL}^1(\text{NO}_3)_3] \cdot \text{H}_2\text{O}$, and the $[\text{EuL}^{2,3}(\text{NO}_3)_3] \cdot \text{H}_2\text{O}$ are the same result, so I won't describe them in detail here.

In order to prove the composition and thermal stability of Eu(III) complexes further, ESI-MS analysis is measured in DMF with 10^{-6} M and the test mode is positive ion mode. Based on the similar structure of all Eu(III) complexes, only $[\text{EuL}^1(\text{NO}_3)_3] \cdot \text{H}_2\text{O}$ is selected for detailed

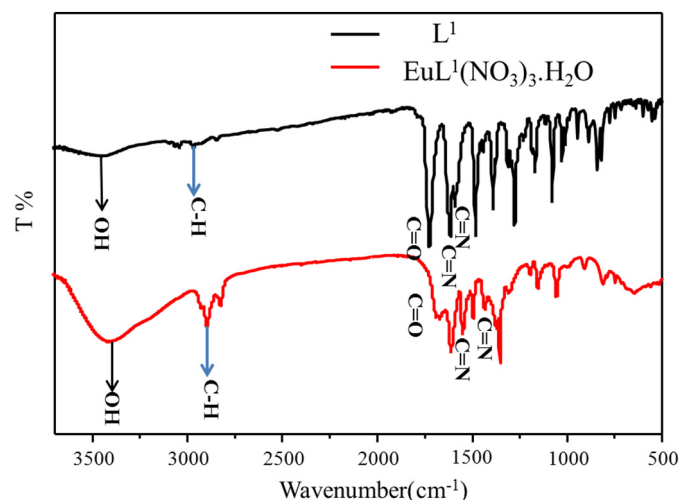


Fig. 2. The FT-IR spectrum of L¹ and $[\text{EuL}^1(\text{NO}_3)_3] \cdot \text{H}_2\text{O}$.

Table 2
Elemental analysis of $[\text{Eu}^{1-3}(\text{NO}_3)_3] \cdot \text{H}_2\text{O}$.

Complexes	Found(calculated)%				
	C	H	N	O	Eu
$[\text{Eu}^1(\text{NO}_3)_3] \cdot \text{H}_2\text{O}$	29.96(30.18)	2.33(2.20)	11.86(11.00)	31.02(30.18)	28.92(28.88)
$[\text{Eu}^2(\text{NO}_3)_3] \cdot \text{H}_2\text{O}$	31.10(30.62)	2.38(2.40)	11.12(10.51)	32.13(31.22)	23.03(22.81)
$[\text{Eu}^3(\text{NO}_3)_3] \cdot \text{H}_2\text{O}$	29.20(28.18)	2.10(1.91)	12.67(12.33)	34.98(35.23)	23.12(22.31)

analysis. ESI-MS data of $[\text{Eu}^{1-3}(\text{NO}_3)_3] \cdot \text{H}_2\text{O}$ are shown in Table 3. The m/z 629.02 $[\text{M} + \text{H}]^+$ can be obviously observed in Fig. 3, which is consistent with the theoretically calculated value (m/z : 628.04) of $[\text{Eu}^1(\text{NO}_3)_3] \cdot \text{H}_2\text{O}$. Meanwhile the m/z 670.04 $[\text{M} + \text{H}]^+$ and 682.96 $[\text{M} + \text{H}]^+$ of $[\text{Eu}^{2,3}(\text{NO}_3)_3] \cdot \text{H}_2\text{O}$ are also can be found in support information, which matches well with the theoretical value of $[\text{Eu}^{2,3}(\text{NO}_3)_3] \cdot \text{H}_2\text{O}$ (m/z : 669.06 and m/z : 681.20).

Besides, the TG analysis of $[\text{Eu}^{1-3}(\text{NO}_3)_3] \cdot \text{H}_2\text{O}$ were investigated in the air atmosphere. Similarly, only $[\text{Eu}^1(\text{NO}_3)_3] \cdot \text{H}_2\text{O}$ is explained in detail here, and the TG experimental data and curve of $[\text{Eu}^1(\text{NO}_3)_3] \cdot \text{H}_2\text{O}$ are exhibited in Table 3 and Fig. 4. The TG curve of $[\text{Eu}^{2,3}(\text{NO}_3)_3] \cdot \text{H}_2\text{O}$ can be viewed in the support information. As we can see from the Table 3 and Fig. 4, the process of the compound losing weight is mainly divided into three steps: (1) loss of crystal water, (2) loss of nitrate (3) the removal of the ligand. Firstly, when the temperature is in the range of 90–110 °C, the weight loss ratio of the $[\text{Eu}^1(\text{NO}_3)_3] \cdot \text{H}_2\text{O}$ is 2.85%, which is consistent with the theoretical value (2.83%) of crystallization water in $[\text{Eu}^1(\text{NO}_3)_3] \cdot \text{H}_2\text{O}$. Secondly, when the temperature is in the range of 110–349 °C, the weight loss ratio of the complex is 29.05%, which is also very close to the theoretical calculated value (29.23%) of nitrate in the complex. Finally, when the temperature rises from 349 °C to 760 °C, the weight loss ratio is 43.05%, which is also close to the theoretical calculation value (44.05%) of the ligand in the complex. The weight loss is completed until 760 °C. When the temperature exceeds 760 °C, the curve begins to stagnate, indicating that the residue corresponds to europium oxide and the residual value (26.30%) is close to the theoretical analysis value (27.19%) [39]. Correspondingly, the peak of 629.0 in the ESI-MS corresponds to the molecular ion peak of $[\text{Eu}^1(\text{NO}_3)_3] \cdot \text{H}_2\text{O}$ (Theoretical relative molecular mass is 630.2), and that is consistent with the results of FT-IR, TG and molar conductivity analysis [40]. All the residue values and the peak of ESI-MS of $[\text{Eu}^{1-3}(\text{NO}_3)_3] \cdot \text{H}_2\text{O}$ are consistent with theoretical values.

3.2.3. Presumed structural formula of $[\text{Eu}^{1-3}(\text{NO}_3)_3] \cdot \text{H}_2\text{O}$

Based on the above FT-IR, molar conductivity, elemental analysis, ESI-MS, and TG analysis, the chemical molecular formula of the Eu(III) complexes can be successfully determined to be $[\text{Eu}^{1-3}(\text{NO}_3)_3] \cdot \text{H}_2\text{O}$, and the structural formula of $[\text{Eu}^{1-3}(\text{NO}_3)_3] \cdot \text{H}_2\text{O}$ is shown in Fig. 5.

3.2.4. Fluorescence properties

The fluorescence performance of the complex was measured in DMSO and the corresponding data was placed in the Fig. 6 and Table 4. The fluorescence quantum yields were calculated according to the above formula ($n_{\text{x(DMSO)}} = 1.478$). The corresponding fluorescence spectrum data was listed in the Table 4. The excitation and emission spectra were shown in Fig. 6. The energy transfer mechanism was shown in Fig. 7.

Table 3
TG and ESI-MS data of $[\text{Eu}^{1-3}(\text{NO}_3)_3] \cdot \text{H}_2\text{O}$.

Complexes	Found (calculated) of lose weight (%)				ESI-MS Found(calcd)
	Crystal water	Nitrate	ligand	Residue	
$[\text{Eu}^1(\text{NO}_3)_3] \cdot \text{H}_2\text{O}$	2.85(2.83)	29.05(29.23)	43.05(44.05)	26.30(27.19)	629.02(628.04)
$[\text{Eu}^2(\text{NO}_3)_3] \cdot \text{H}_2\text{O}$	3.00(2.70)	27.00(27.92)	44.50(46.57)	25.50(25.96)	670.04(669.06)
$[\text{Eu}^3(\text{NO}_3)_3] \cdot \text{H}_2\text{O}$	2.79(2.64)	27.20(27.30)	43.80(47.75)	25.20(25.39)	682.96(681.20)

As shown in Figs. 6 and 7, the maximum excitation wavelengths of the three complexes are all located at 393 nm, and the corresponding excitation intensity order is $[\text{Eu}^2(\text{NO}_3)_3] \cdot \text{H}_2\text{O} > [\text{Eu}^1(\text{NO}_3)_3] \cdot \text{H}_2\text{O} > [\text{Eu}^3(\text{NO}_3)_3] \cdot \text{H}_2\text{O}$. All the complexes emit the red characteristic fluorescence of Eu(III). Three target complexes show obvious emission peaks at 595 nm and 618 nm, and lower emission peaks appeared at 651 nm and 701 nm, which mainly correspond to the $^5\text{D}_0$ - $^7\text{F}_1$, $^5\text{D}_0$ - $^7\text{F}_2$, $^5\text{D}_0$ - $^7\text{F}_3$ and $^5\text{D}_0$ - $^7\text{F}_4$ transitions. This indicates that ligands are successfully coordinated with Eu(III). Correspondingly, $^5\text{D}_0 \rightarrow ^7\text{F}_1$ and $^5\text{D}_0 \rightarrow ^7\text{F}_2$ transitions are located at 595 nm and 618 nm, which are attributed to magnetic dipole transitions and electric dipole transitions, respectively [41]. Like many Eu(III) complex materials, the Stokes shift of above materials is up to 225 nm. Generally, the symmetric positional information of the Eu(III) in the complexes is mainly judged by the intensity ratio of $^5\text{D}_0 \rightarrow ^7\text{F}_1$ and $^5\text{D}_0 \rightarrow ^7\text{F}_2$ transitions. The fluorescence intensity ratio η ($^5\text{D}_0 \rightarrow ^7\text{F}_2/5\text{D}_0 \rightarrow ^7\text{F}_1$) of the two orbits is an important indicator for judging the symmetrical position of Eu(III). When the η are more than 1, the $^5\text{D}_0 \rightarrow ^7\text{F}_2$ electric dipole transition emits red light (618 nm). At this time, Eu(III) is in a position away from the inversion center. When the η are less than 1, the $^5\text{D}_0 \rightarrow ^7\text{F}_1$ magnetic dipole transition emits orange light (596 nm). At this time, Eu(III) is in the lattice position close to the inversion center. The η values of the above three target complexes are all larger than 1, which indicates that the europium ions in these three complexes are all located away from the inversion center, that is, the asymmetric center [42].

Obviously, the fluorescence intensity and the fluorescence quantum yields of $[\text{Eu}^2(\text{NO}_3)_3] \cdot \text{H}_2\text{O}$ is higher than $[\text{Eu}^1(\text{NO}_3)_3] \cdot \text{H}_2\text{O}$, while the fluorescence intensity and the fluorescence quantum yields of $[\text{Eu}^3(\text{NO}_3)_3] \cdot \text{H}_2\text{O}$ is lower than $[\text{Eu}^1(\text{NO}_3)_3] \cdot \text{H}_2\text{O}$. These indicate that the introduction of electron-donating groups can enhance the fluorescence intensity of Eu complexes, while the introduction of electron-withdrawing groups can weaken the fluorescence intensity of Eu complexes. This is mainly because the introduction of an electron-donating group increases the conjugation of molecules and the density of electron clouds, which promotes the energy transfer efficiency between the ligand and the characteristic ions. In other words, there will be more electrons in the ligand entering the empty orbit of the rare earth ions as the electron donating capacity increases, which further illustrates that the electron-donating group can improve the fluorescence properties of the complexes.

To study the effect of different substituents on the fluorescence intensity of the complexes, the density functional theory (DFT) calculation of L^{1-3} was performed with Gaussian 09 program [43–45]. The geometries were optimized by the B3LYP hybrid density functional and the basis set was 6-31G (d). The frontier molecular orbitals and energy levels of the highest occupied molecular orbital (HOMO) and lowest unoccupied molecular orbital (LUMO) of L^{1-3} are shown in Fig. 8, and the

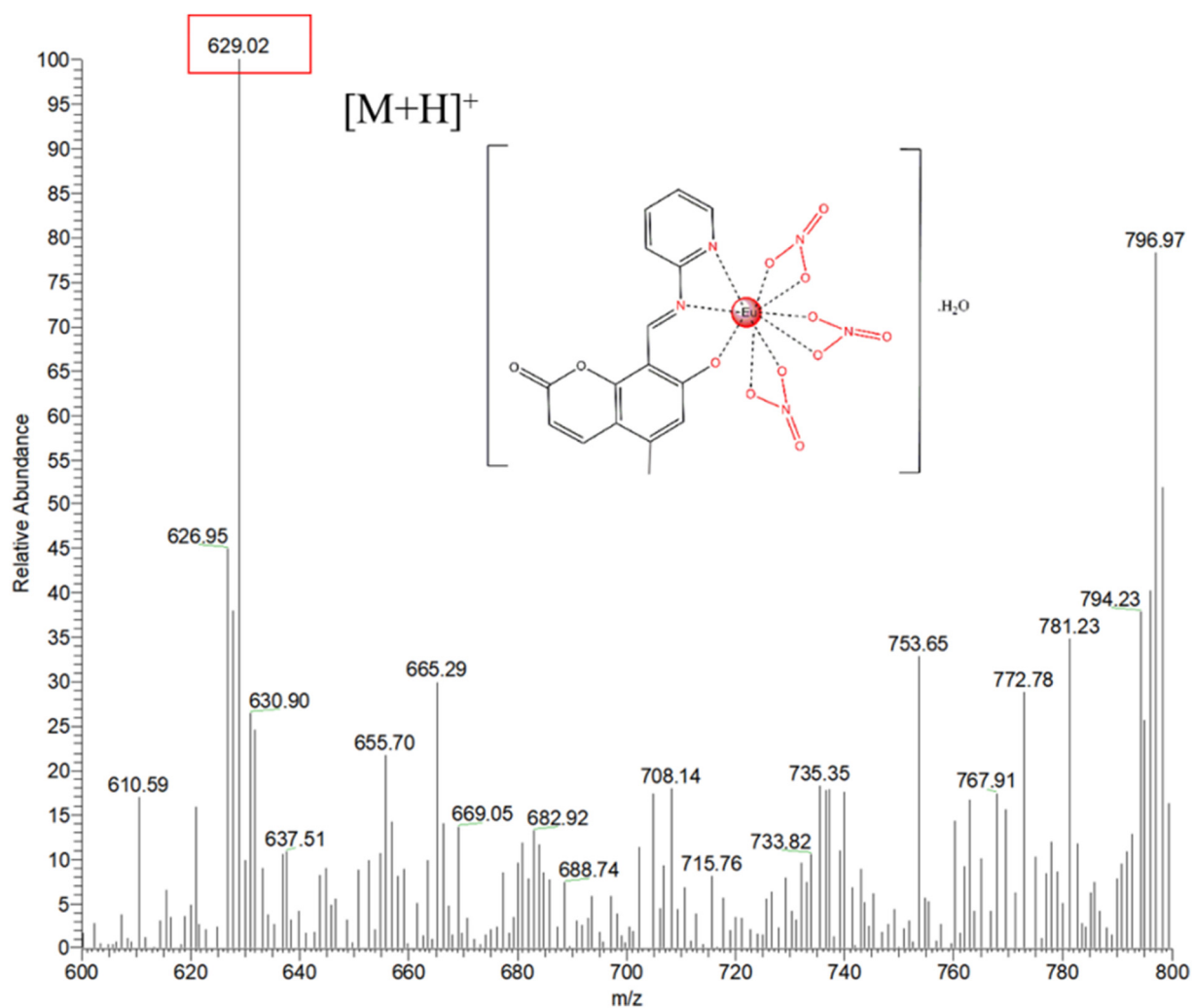


Fig. 3. The ESI-MS spectrum of $[EuL(NO_3)_3] \cdot H_2O$.

calculated HOMO and LUMO energy level and corresponding energy gaps (Eg) are listed.

It can be seen from Fig. 8, the electron density distribution in orbital of L^{1-3} suggests that the HOMOs are extended over almost all the

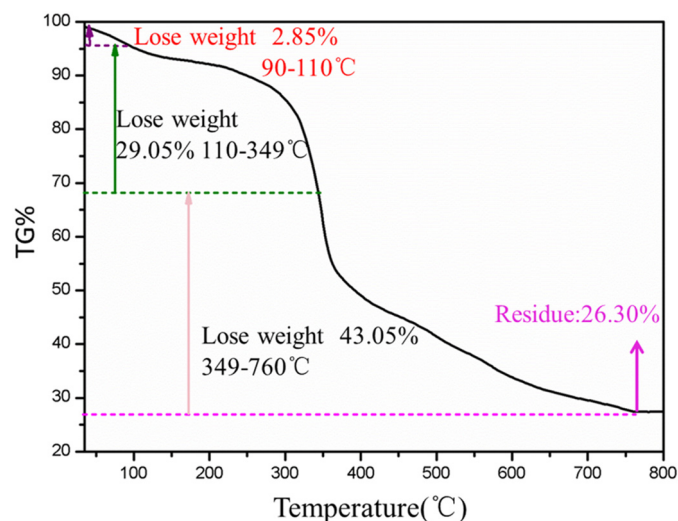


Fig. 4. The TG curves of $[EuL(NO_3)_3] \cdot H_2O$.

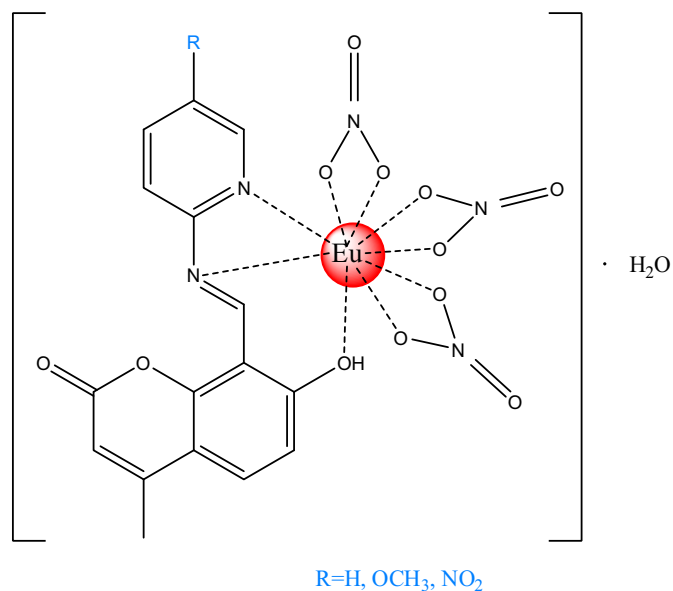


Fig. 5. The structural formula of $[EuL^{1-3}(NO_3)_3] \cdot H_2O$.

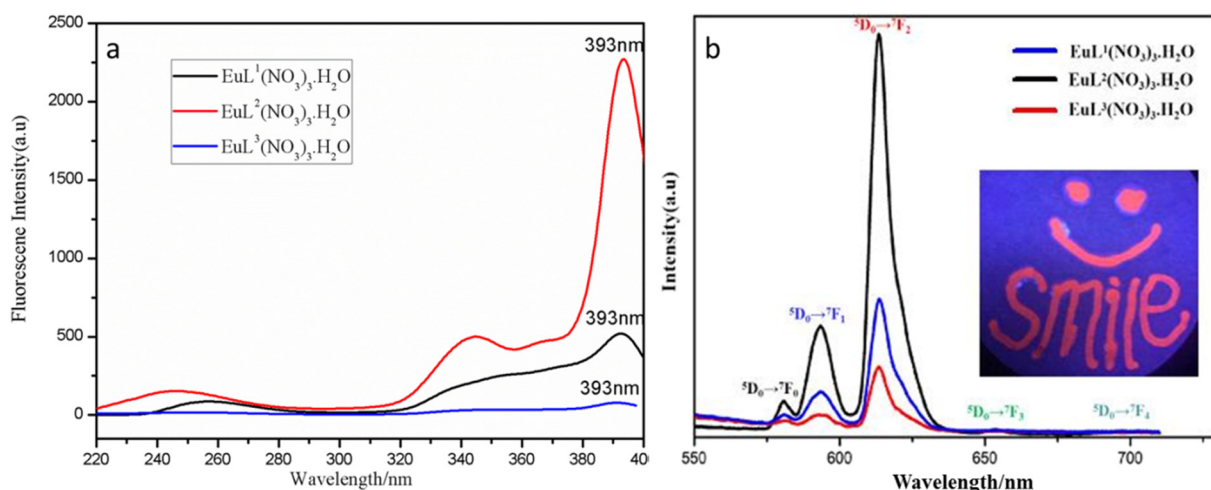


Fig. 6. (a) Excitation spectrum of $[\text{EuL}^{1-3}(\text{NO}_3)_3]\cdot\text{H}_2\text{O}$ (b) Emission spectrum of $[\text{EuL}^{1-3}(\text{NO}_3)_3]\cdot\text{H}_2\text{O}$.

molecule excepting the substituent groups (Methyl group, C=O or C=C). Compared with L^1 (LUMO: -1.91 eV, HOMO: -5.96 eV), the strong electron-donating substituent $-\text{OCH}_3$ on pyridine ring (L^2) increases the LUMO energy level (-1.82 eV) and the HOMO energy level (-5.58 eV). However, the strong electron-withdrawing substituent $-\text{NO}_2$ on pyridine ring (L^3) decreases the LUMO energy level (-2.68 eV) and the HOMO energy level (-6.45 eV). Compared with the HOMO energy level of L^{1-3} , the electron-donating group ($-\text{OCH}_3$) increases the HOMO energy level of the ligand (L^2), that is, the electron cloud density is enhanced, and it is concentrated in the pyridine ring (including C=N participating in the coordination), C=N double bond and benzene ring (including hydroxyl groups), which makes the ligand more likely to undergo electronic transition after coordination with europium ions, and the conjugation of the corresponding complex is enhanced, so the fluorescence intensity is relatively strong. The introduction of electron-withdrawing group ($-\text{NO}_2$) makes the fluorescence intensity of the complex have different result, that is, the fluorescence intensity is weakened. As can be seen from Fig. 8, this is because the introduction of electron-withdrawing group ($-\text{NO}_2$) reduces its HOMO energy level, which reduces the density of the electron cloud around the coordination functional group. Based on the above analysis, substituents on pyridine ring have a great influence on the electronic cloud distribution of the molecule, which leads to different fluorescence intensity emission of $[\text{EuL}^{1-3}(\text{NO}_3)_3]\cdot\text{H}_2\text{O}$. This may be an effective reference for the design of excellent ligands in the field of optical materials.

3.2.5. Electrochemical properties

The cyclic voltammetry curves (CV) of the $[\text{EuL}^{1-3}(\text{NO}_3)_3]\cdot\text{H}_2\text{O}$ were measured at the electrochemical workstation. The lowest unoccupied orbital energy level (LUMO) of the Eu(III) complexes, the highest occupied orbital energy level (HOMO) and the oxidation potential E_{OX} were investigated. The HOMO energy level can be calculated by the formula $E_{\text{HOMO}} = -(4.74 + E_{\text{OX}})$ eV, and the corresponding LUMO energy level can be obtained by the formula $E_{\text{LUMO}} = E_{\text{HOMO}} + E_g$, E_g is calculated by the formula $E_g = 1240/\lambda_{\text{onset}}$ (eV). E_{OX} is measured by the

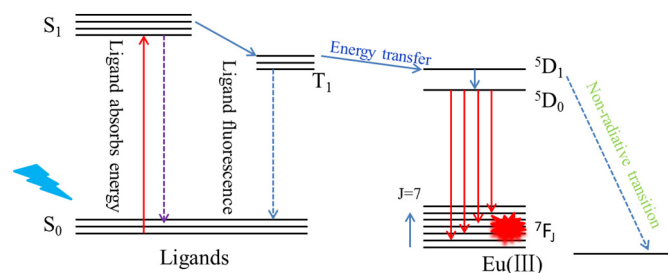


Fig. 7. Energy transfer mechanism of $[\text{EuL}^{1-3}(\text{NO}_3)_3]\cdot\text{H}_2\text{O}$.

cyclic voltammetry and λ_{onset} is the starting value of the maximum absorption peak of the ultraviolet absorption spectrum [46,47].

As shown in Fig. 9 and Table 5, the maximum ultraviolet absorption wavelengths (λ_{onset}) of the three target complexes are 343 nm, 339 nm and 342 nm, respectively. The oxidation potential (E_{OX}) of Eu(III) complexes is found in the range of 0.6935–0.7762. Compared with $[\text{EuL}^1(\text{NO}_3)_3]\cdot\text{H}_2\text{O}$ (LUMO: -1.8265 eV, HOMO: -5.4417 eV, E_g : 3.6152), the electron-donating substituent $-\text{OCH}_3$ on $[\text{EuL}^2(\text{NO}_3)_3]\cdot\text{H}_2\text{O}$ increases the LUMO energy level (-1.7757 eV), HOMO energy level (-5.4335 eV) and the E_g value (3.6578 eV). However, the effect of introducing electron withdrawing groups is opposite to that of electron-donating groups. The E_g value of the three target Eu(III) complexes are relatively high (all around 3.65), which means that all target Eu(III) complexes have a good chemical stability. This indicates that more electrons in $[\text{EuL}^2(\text{NO}_3)_3]\cdot\text{H}_2\text{O}$ enter the empty orbital of the Eu^{3+} , a larger conjugated structure is formed, and the chemical stability and fluorescence intensity are enhanced.

3.3. Ion detection performance

3.3.1. Ion-selective analysis of Eu(III) complexes

By comparing the fluorescence properties of the three complexes, we selected $[\text{EuL}^2(\text{NO}_3)_3]\cdot\text{H}_2\text{O}$ to conduct anion selectivity

Table 4
Fluorescence intensity of $[\text{EuL}^{1-3}(\text{NO}_3)_3]\cdot\text{H}_2\text{O}$.

Compounds	λ_{ex} (nm)	$^5\text{D}_0-^7\text{F}_1$		$^5\text{D}_0-^7\text{F}_2$		Φ_{fx}	η ($^5\text{D}_0-^7\text{F}_2/^5\text{D}_0-^7\text{F}_1$)
		$\lambda_{\text{em}}/\text{nm}$	I/a.u.	$\lambda_{\text{em}}/\text{nm}$	I/a.u.		
$[\text{EuL}^1(\text{NO}_3)_3]\cdot\text{H}_2\text{O}$	393	596	502	618	1645	0.189	3.28
$[\text{EuL}^2(\text{NO}_3)_3]\cdot\text{H}_2\text{O}$	393	595	1134	618	4929	0.533	4.35
$[\text{EuL}^3(\text{NO}_3)_3]\cdot\text{H}_2\text{O}$	393	595	325	618	896	0.105	2.76

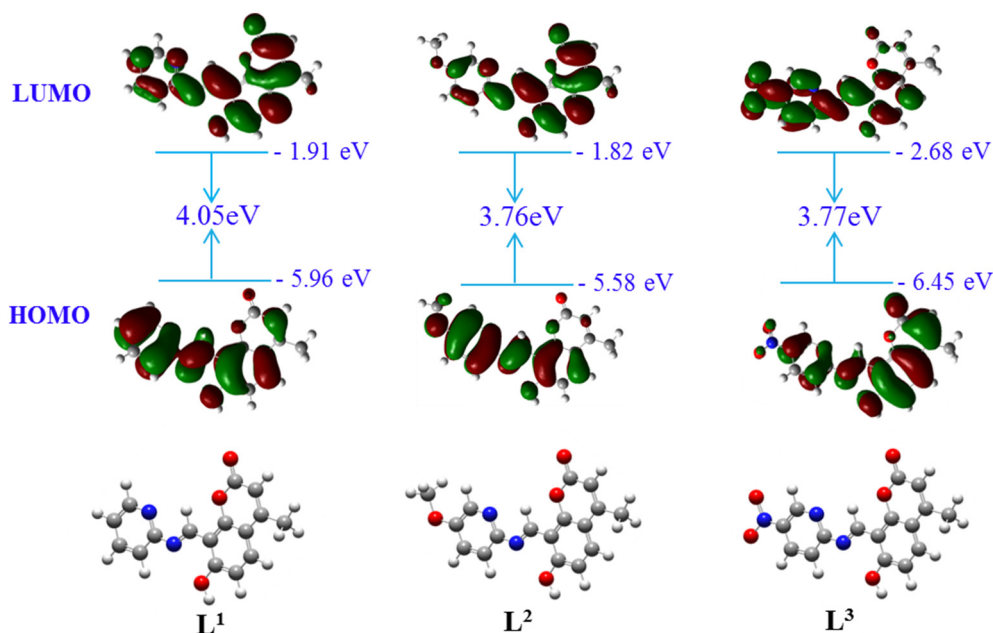


Fig. 8. Optimized molecular structure and molecular orbital amplitude plots of HOMO and LUMO energy level of L^{1-3} .

experiments due to its excellent fluorescence performance. In order to explore the anions specifically recognized by this complex, F^- , Cl^- , Br^- , I^- , SO_4^{2-} , NO_3^- and blank control samples were selected for selective experiments. This selective experiment was conducted under the condition of DMSO/ H_2O (V/V) = 8:2, and the test concentration was $1.0 \times 10^{-4} \text{ mol} \cdot L^{-1}$. The selective fluorescence curve is shown in Fig. 8.

It can be seen from Fig. 10, when Cl^- , Br^- , I^- , SO_4^{2-} , and NO_3^- are added, the fluorescence intensity of the Eu(III) characteristic fluorescence of $[EuL^2(NO_3)_3] \cdot H_2O$ all changes significantly. The fluorescence intensity of the ${}^5D_0-{}^7F_1$ and ${}^5D_0-{}^7F_2$ transitions is continuously decreased, and there is no obvious change in the fluorescence peak around 455 nm. And the fluorescence intensity of the complex solution at 595 nm and 620 nm is always higher than the broad fluorescence peak around 455 nm, which shows that the fluorescence of the complex solution is still dominated by the red characteristic fluorescence of europium ion at this time. In other words, there is no obvious fluorescence color change, that is, the complex has no specific recognition function

Table 5

The electrochemical data of complexes.

Compounds	λ_{onset} (nm)	Eox (V)	E_{HOMO} (eV)	Eg (eV)	E_{LUMO} (eV)
$EuL^1(NO_3)_3 \cdot 2H_2O$	343	0.7017	-5.4417	3.6152	-1.8265
$EuL^2(NO_3)_3 \cdot 2H_2O$	339	0.6935	-5.4335	3.6578	-1.7757
$EuL^3(NO_3)_3 \cdot 2H_2O$	342	0.7762	-5.5162	3.6257	-2.1163

for these anions. When F^- is added, the apparent color of the solution becomes turbid from the colorless transparent solution. The fluorescence intensity of the complex at 455 nm increased rapidly, the fluorescence intensity at 595 nm and 620 nm decreased sharply, and the solution showed a blue fluorescent around 455 nm, which shows that the complex has a specific recognition function for F^- . Since the ligand is coordinated by two $-C=N$ and $-OH$ with Eu^{3+} to form a metal chemical bond, in general, the five-membered ring and the six-membered ring are more stable, while the two $C=N$ and Eu^{3+} are formed the

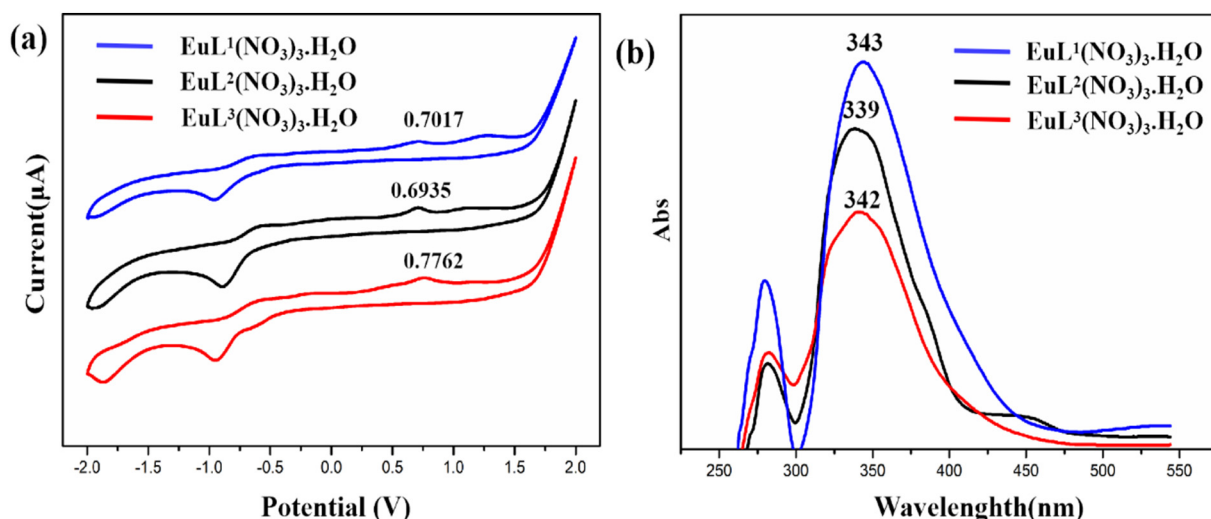


Fig. 9. (a) The cyclic voltammetry curves (CV) of Eu complexes (b) The UV-Vis spectrum of Eu complexes.

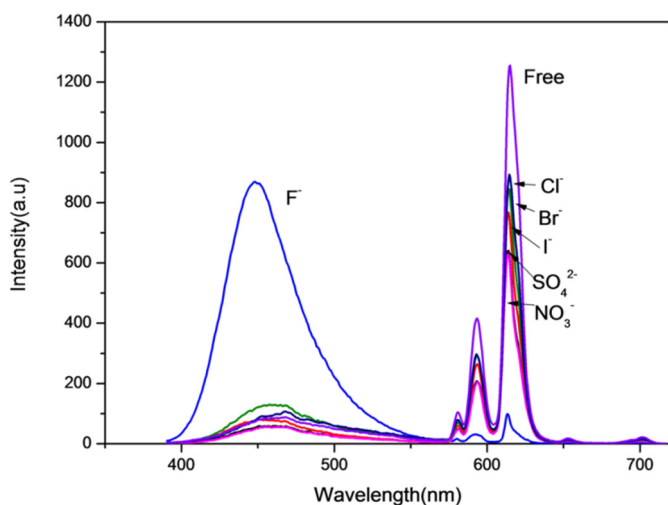


Fig. 10. Fluorescence spectra of the complex solution under the same amount of different anions.

four-membered ring is not very stable. When F^- is added, F^- is more likely to combine with Eu^{3+} to generate europium fluoride. The new bond of the complex is broken, that is, the existing structure of the complex is destroyed. Therefore, the characteristic fluorescence intensity of $Eu(III)$ complex is significantly reduced. This selective experiment shows that $[EuL^2(NO_3)_3] \cdot H_2O$ possesses a specific recognition function for F^- , which also shows that the complex has a potential application prospects in the field of ion detection.

3.3.2. Response range of $Eu(III)$ complex to F^- detection

Through the anion selectivity experiment, we found that the complex has a specific recognition function for F^- , and further explore the detection range of the complex for F^- , the experimental condition is $DMSO/H_2O(V/V) = 8:2$. The concentration of the complex is $1.0 \times 10^{-4} \text{ mol} \cdot L^{-1}$, and the ion concentration is controlled at $0.0\text{--}3.0 \times 10^{-5} \text{ mol} \cdot L^{-1}$. The fluorescence intensity data of the complex solution at different F^- concentrations are shown in Table 6. The corresponding fluorescence spectrum is shown in Fig. 10.

It can be seen from the above Fig. 11 and Table 6, through the continuous increase of the concentration of F^- , the fluorescence intensity of the complex solution at 455 nm continues to increase, and the fluorescence intensity of the complex at 620 nm continues to decrease, which shows that the complex has a good recognition function and high sensitivity of response to F^- . When the concentration of F^- is in the range of $2.0 \times 10^{-6} \text{ mol} \cdot L^{-1}$ to $8.0 \times 10^{-6} \text{ mol} \cdot L^{-1}$, the fluorescence intensity of the complex at 620 nm is significantly higher than that at 455 nm, namely $I_{455nm}/I_{620nm} < 1$. and the complex exhibits

Table 6
Fluorescence intensity data of different F^- concentrations in complex solution.

Concentration (F^-)/M	Wavelength/nm	I/a.u.	Wavelength/nm	I/a.u.
2.0×10^{-6}	455	26	620	631
4.0×10^{-6}	455	42	620	530
6.0×10^{-6}	455	89	620	482
8.0×10^{-6}	455	188	620	439
1.0×10^{-5}	455	712	620	421
1.2×10^{-5}	455	1035	620	392
1.4×10^{-5}	455	3761	620	384
1.6×10^{-5}	455	4629	620	361
1.8×10^{-5}	455	5134	620	258
2.0×10^{-5}	455	6892	620	247
2.2×10^{-5}	455	7719	620	129
2.4×10^{-5}	455	7732	620	121
2.6×10^{-5}	455	7739	620	120
2.8×10^{-5}	455	7742	620	58

characteristic red fluorescence in this concentration range of F^- . At this time, the detection sensitivity of the complex to F^- is weak. With the increasing concentration of F^- , when the concentration of F^- reaches $1.0 \times 10^{-5} \text{ mol} \cdot L^{-1}$, at this time, $I_{455nm}/I_{620nm} > 1$, the fluorescence at 455 nm wavelength becomes dominant, and the complex mainly emits blue fluorescence, that is, the detection of the complex to F^- reached a critical value. When the concentration increased from $1.2 \times 10^{-5} \text{ mol} \cdot L^{-1}$ to $1.6 \times 10^{-5} \text{ mol} \cdot L^{-1}$, the fluorescence intensity of the solution showed a sharp increase, and the fluorescence intensity reached 3761. Then as the fluoride ion continue increases, the ratio of I_{455nm}/I_{620nm} increases linearly. When the concentration reaches $2.2 \times 10^{-5} \text{ mol} \cdot L^{-1}$, the ratio of I_{455nm}/I_{620nm} no longer increases, which indicates that the maximum response range of the complex has been reached, and the response sensitivity of the complex is between $1.0 \times 10^{-5} \text{ mol} \cdot L^{-1}$ and $2.2 \times 10^{-5} \text{ mol} \cdot L^{-1}$. This is because with the continuous increase of F^- , the new bond formed is broken, that is, the structure of the complex is destroyed, and the fluorescence intensity of the complex in the characteristic wavelength region of europium ions decreases. When the concentration of F^- increases to a certain value, the complex no longer responds, this indicates that the response limit has been reached at this concentration. The above ion selectivity experiments and F^- quantitative exploration indicate that the target $Eu(III)$ complex has certain application potential in the detection of F^- .

4. Conclusions

In summary, three novel coumarin derivatives and corresponding $Eu(III)$ complexes were synthesized and characterized by 1H NMR, ^{13}C NMR, UV-Vis, FT-IR, ESI-MS, TG, elemental analysis and molar conductivity. All the ligands exhibit the AIE property in CH_3CN/H_2O solution and emit green fluorescence with the maximum emission wavelength of 552 nm. All the $Eu(III)$ complexes show characteristic red fluorescence of $Eu(III)$ and the influence of different substituents on the fluorescence intensity of $Eu(III)$ complexes is ordered: $-OCH_3 > -H > -NO_2$, and $[EuL^2(NO_3)_3] \cdot H_2O$ shows the strongest fluorescence intensity. The density functional theory (DFT) calculations of the ligands indicate that the introduction of electron-donating groups increases the HOMO energy level and the electron cloud density, which enhance the ability of ligand to coordinate with $Eu(III)$ and the fluorescence intensity of the corresponding $Eu(III)$ complex. Besides, the electrochemical properties of $Eu(III)$ complexes indicate that the introduction of electron-donating groups increases the energy gaps (E_g) and the conjugation of the complex, which enhances the fluorescence intensity of the complex. Ion selectivity experiments show that $[EuL^2(NO_3)_3] \cdot H_2O$ has a specific recognition function for F^- , and its response limit is between $1.0 \times 10^{-5} \text{ mol} \cdot L^{-1}$ and $2.2 \times 10^{-5} \text{ mol} \cdot L^{-1}$. Compared with other reported coumarin Schiff base derivatives [48–51], the ligands L^{1-3} synthesized in this work possess outstanding AIE properties and emit strong green fluorescence, which have great application prospects in the field of optical materials. Besides, the $[EuL^{1-3}(NO_3)_3] \cdot H_2O$ synthesized in this work show excellent fluorescence property and $[EuL^2(NO_3)_3] \cdot H_2O$ has the strongest fluorescence intensity. What's more interesting is that $[EuL^2(NO_3)_3] \cdot H_2O$ is selective for F^- , and its response limit is between $1.0 \times 10^{-5} \text{ mol} \cdot L^{-1}$ and $2.2 \times 10^{-5} \text{ mol} \cdot L^{-1}$, which indicates the $Eu(III)$ complex has potential application prospects in the field of fluoride ion detection. This provides a new idea for the application of rare earth complexes based on coumarin Schiff base derivatives for our group, and also provides a direction for subsequent research work.

CRedit authorship contribution statement

Fangfei Luan: Conceptualization, Formal analysis, Investigation, Methodology, Project administration, Software, Visualization, Writing - Original Draft, Writing - review & editing. **Gangxiang Xiao:** Formal analysis, Investigation, Methodology, Validation, Writing - review &

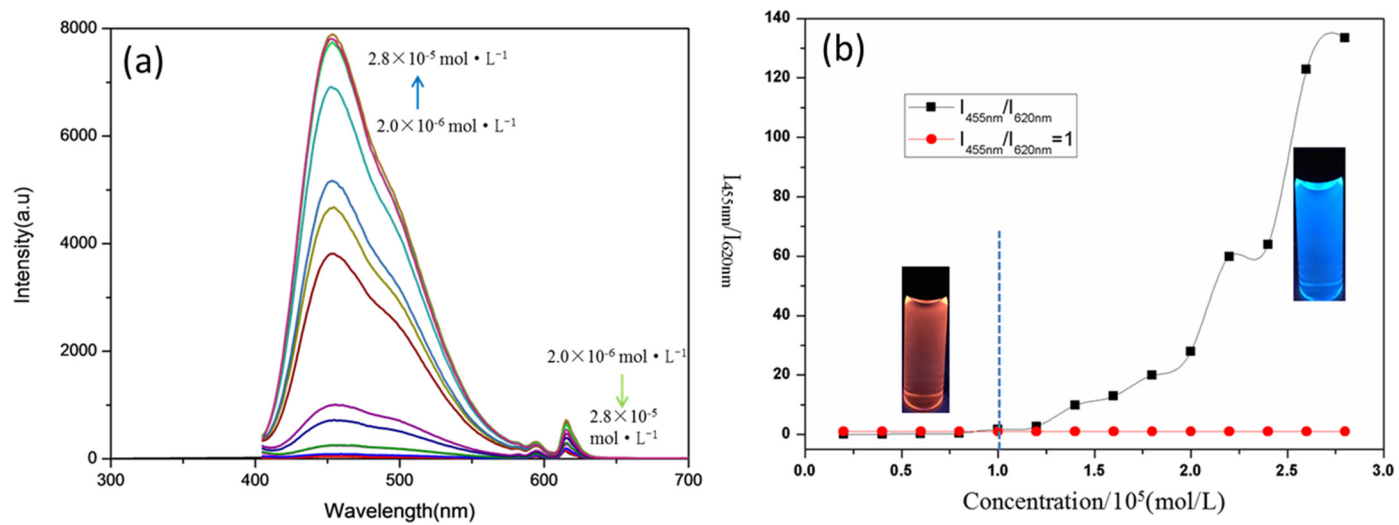


Fig. 11. (a) Fluorescence spectra of complex solution at different concentrations of F^- (b) The curve of the ratio of $I_{455\text{nm}}/I_{620\text{nm}}$ with the concentration of F^- .

editing. **Yuxi Zhang**: Data curation, Investigation, Methodology, Writing - review & editing. **Shiquan Li**: Data curation, Investigation, Methodology, Writing - review & editing. **Zhongqian Hu**: Formal analysis, Validation, Writing - review & editing. **Hongli Du**: Validation, Writing - review & editing. **Dongcai Guo**: Conceptualization, Resources, Supervision, Validation, Funding acquisition.

Declaration of competing interest

The authors declared that they have no conflicts of interest to this work.

We declare that we do not have any commercial or associative interest that represents a conflict of interest in connection with the work submitted.

Acknowledgments

The authors are grateful for the financial support of the National Natural Science Foundation of China (No. 21341010), Hunan Provincial Science and Technology Department (No. 2016SK2064). We also thank Dr. William Hickey, the U.S. professor of HRM, for the English editing on this paper.

Appendix A. Supplementary data

Supplementary data to this article can be found online at <https://doi.org/10.1016/j.molliq.2020.114439>.

References

- I. Cota, V. Marturano, B. Tylkowski, Ln complexes as double faced agents: study of antibacterial and antifungal activity, *Coord. Chem. Rev.* 396 (2019) 49–71, <https://doi.org/10.1016/j.ccr.2019.05.019>.
- R. Pelc, P. Bour, Spectral Counterstaining in Luminescence-enhanced Biological Raman Microscopy *†*, 2019 8329–8332, <https://doi.org/10.1039/c9cc03139a>.
- L. Jiang, W. Chen, J. Zheng, L. Zhu, L. Mo, Z. Li, L. Hu, T. Hayat, A. Alsaedi, C. Zhang, S. Dai, Enhancing the Photovoltaic Performance of Perovskite Solar Cells With a Down-conversion Eu-complex, 2017 3–9, <https://doi.org/10.1021/acsami.7b10101>.
- L.F. Chiriac, P.C. Ganea, D.M. Maximean, I. Pasuk, V. Cîrcu, Synthesis and thermal, emission and dielectric properties of liquid crystalline Eu(III), Sm(III) and Tb(III) complexes based on mesogenic 4-pyridone ligands functionalized with cyanobiphenyl groups, *J. Mol. Liq.* 290 (2019), 111184, <https://doi.org/10.1016/j.molliq.2019.111184>.
- G. Qiao, Z. Lai, J. Gao, W. Liu, Y. Zheng, Lanthanide molecular model triggers sequential sensing performance, *J. Mol. Liq.* 311 (2020), 113344, <https://doi.org/10.1016/j.molliq.2020.113344>.
- M.W. Mara, D.S. Tatum, A.M. March, G. Doumy, E.G. Moore, K.N. Raymond, Energy transfer from antenna ligand to europium(III) followed using ultrafast optical and X-ray spectroscopy, *J. Am. Chem. Soc.* 141 (2019) 11071–11081, <https://doi.org/10.1021/jacs.9b02792>.
- J. Kang, J. Yu, A. Li, D. Zhao, B. Liu, L. Guo, B. Tang, Amorphous Ag₂S micro-rods-enhanced fluorescence on liquid crystals: cation- π interaction-triggered aggregation-induced emission effect, *iScience* 15 (2019) 119–126, <https://doi.org/10.1016/j.isci.2019.04.017>.
- Y. Zhang, W. Xu, L. Kong, B. Han, Z. Cai, J. Shi, B. Tong, Y. Dong, B. Tang, Turn-on fluorescent probe with aggregation-induced emission characteristics for polyazoles, *Mater. Chem. Front.* 2 (2018) 1779–1783, <https://doi.org/10.1039/c8qm00235e>.
- J. Qiu, K. Wang, Z. Lian, X. Yang, W. Huang, A. Qin, Q. Wang, J. Tian, B. Tang, S. Zhang, Prediction and understanding of AIE effect by quantum mechanics-aided machine-learning algorithm, *Chem. Commun.* 54 (2018) 7955–7958, <https://doi.org/10.1039/c8cc02850h>.
- Q. Feng, Y. Li, L. Wang, C. Li, J. Wang, Y. Liu, K. Li, H. Hou, Multiple-color aggregation-induced emission (AIE) molecules as chemodosimeters for pH sensing, *Chem. Commun.* 52 (2016) 3123–3126, <https://doi.org/10.1039/c5cc10423h>.
- C. Zhu, S. Pang, J. Xu, L. Jia, F. Xu, J. Mei, A. Qin, J. Sun, J. Ji, B. Tang, Aggregation-induced emission of tetraphenylethene derivative as a fluorescence method for probing the assembling/disassembling of amphiphilic molecules, *Analyst* 136 (2011) 3343–3348, <https://doi.org/10.1039/c1an15176b>.
- A. Sen Gupta, K. Paul, V. Luxami, A fluorescent probe with “AIE + ESIPT” characteristics for Cu²⁺ and F[−] ions estimation, *Sensors Actuators B Chem.* 246 (2017) 653–661, <https://doi.org/10.1016/j.snb.2017.02.080>.
- D. Xu, M. Liu, H. Zou, J. Tian, H. Huang, Q. Wan, Y. Dai, Y. Wen, X. Zhang, Y. Wei, A new strategy for fabrication of water dispersible and biodegradable fluorescent organic nanoparticles with AIE and ESIPT characteristics and their utilization for bioimaging, *Talanta* 174 (2017) 803–808, <https://doi.org/10.1016/j.talanta.2017.07.010>.
- Y. Dong, J. Shen, W. Li, R. Zhao, Y. Pan, Q. Song, C. Zhang, Opposite ESIPT characteristic of two AIE-active isomers with different linkage sites, *Tetrahedron* 75 (2019) 2670–2675, <https://doi.org/10.1016/j.tet.2019.03.041>.
- M.T. Kaczmarek, M. Zabiszak, M. Nowak, R. Jastrzab, Lanthanides: Schiff base complexes, applications in cancer diagnosis, therapy, and antibacterial activity, *Coord. Chem. Rev.* 370 (2018) 42–54, <https://doi.org/10.1016/j.ccr.2018.05.012>.
- X. Liu, J.R. Hamon, Recent developments in penta-, hexa- and heptadentate Schiff base ligands and their metal complexes, *Coord. Chem. Rev.* 389 (2019) 94–118, <https://doi.org/10.1016/j.ccr.2019.03.010>.
- Y. Hu, W. Chen, Y. Shen, B. Zhu, G.X. Wang, Synthesis and antiviral activity of coumarin derivatives against infectious hematopoietic necrosis virus, *Bioorg. Med. Chem. Lett.* 29 (2019) 1749–1755, <https://doi.org/10.1016/j.bmcl.2019.05.019>.
- J.R. Hwu, W.C. Huang, S.Y. Lin, K.T. Tan, Y.C. Hu, F.K. Shieh, S.O. Bachurin, A. Ustyugov, S.C. Tsay, Chikungunya virus inhibition by synthetic coumarin-guanosine conjugates, *Eur. J. Med. Chem.* 166 (2019) 136–143, <https://doi.org/10.1016/j.ejmech.2019.01.037>.
- H. Yang, X. Chen, J. Wu, R. Wang, H. Yang, A novel up-conversion fluorescence resonance energy transfer sensor for the high sensitivity detection of coumarin in cosmetics, *Sensors Actuators B Chem.* 290 (2019) 656–665, <https://doi.org/10.1016/j.snb.2019.04.014>.
- G. Xiao, M. Li, F. Luan, S. Li, G. Li, Y. Kuang, D. Guo, Multifunctional AIE Schiff-base ligands and corresponding europium(III) complexes: pH response and fluorescence properties, *Dyes Pigments* 168 (2019) 84–92, <https://doi.org/10.1016/j.dyepig.2019.04.032>.
- D. Li, S. Xiong, T. Guo, D. Shu, H. Xiao, G. Li, D. Guo, Novel pyrazolone derivatives and corresponding europium(III) complexes: synthesis and properties research, *Dyes Pigments* 158 (2018) 28–35, <https://doi.org/10.1016/j.dyepig.2018.05.020>.
- M. Dai, H. Xiao, C. Ye, D. Shu, L. Shi, D. Guo, Synthesis and luminescence properties of terbium complexes based on 4-acyl pyrazolone derivatives, *J. Lumin.* 188 (2017) 223–229, <https://doi.org/10.1016/j.jlumin.2017.04.018>.
- W. Zhang, W. He, X. Guo, Y. Chen, L. Wu, D. Guo, Synthesis and luminescence properties of 1,3,4-oxadiazole acetamide derivatives and their rare earth complexes, *J. Alloys Compd.* 620 (2015) 383–389, <https://doi.org/10.1016/j.jallcom.2014.09.153>.
- Y. Ci, X. Ji, Determination of relative fluorescence quantum yields using a simplified method, *Chin. J. Anal. Chem.* 14 (1986) 616–618.
- C. Sun, H. Li, H. Yin, Y. Li, Y. Shi, Effects of the cyano substitution at different positions on the ESIPT properties of alizarin: a DFT/TD-DFT investigation, *J. Mol. Liq.* 269 (2018) 650–656, <https://doi.org/10.1016/j.molliq.2018.08.087>.
- H. Okamoto, K. Itani, M. Yamaji, H. Konishi, H. Ota, Excited-state intramolecular proton transfer (ESIPT) fluorescence from 3-amidophthalimides displaying RGBY emission in the solid state, *Tetrahedron Lett.* 59 (2018) 388–391, <https://doi.org/10.1016/j.tetlet.2017.12.049>.
- D. Jacquemin, M. Khelladi, A. De Nicola, G. Ulrich, Turning ESIPT-based triazine fluorophores into dual emitters: from theory to experiment, *Dyes Pigments* 163 (2019) 475–482, <https://doi.org/10.1016/j.dyepig.2018.12.023>.
- M.C. Dalmolin, C.E. da Silva, C.E. Lunelli, S. Zaionex, P.V. Farago, S.F. Zawadzki, Modified β -cyclodextrin/amidolipine inclusion complexes: preparation and application in aqueous systems, *J. Mol. Liq.* 276 (2019) 531–540, <https://doi.org/10.1016/j.molliq.2018.11.116>.
- L. Bian, J. Nie, H. Dong, L. Zhang, W. Li, H. Zou, T. Huo, F. Dong, M. Song, P. He, X. Nie, M. Chen, S. Chen, S. Sun, H. He, L. Feng, Self-assembly of water-soluble glutathione thiol-capped n-hematite-p-XZn-ferrites (X = Mg, Mn, or Ni): experiment and theory, *J. Phys. Chem. C* 121 (2017) 24046–24059, <https://doi.org/10.1021/acs.jpcc.7b07000>.
- N. Raman, R. Jeyamurugan, S. Sudharsan, K. Karuppasamy, L. Mitu, Metal based pharmacologically active agents: synthesis, structural elucidation, DNA interaction, in vitro antimicrobial and in vitro cytotoxic screening of copper(II) and zinc(II) complexes derived from amino acid based pyrazolone derivatives, *Arab. J. Chem.* 6 (2013) 235–247, <https://doi.org/10.1016/j.arabjc.2012.04.010>.
- M.A. Hussien, N. Nawar, F.M. Radwan, N.M. Hosny, Spectral characterization, optical band gap calculations and DNA binding of some binuclear Schiff-base metal complexes derived from 2-amino-ethanoic acid and acetylacetone, *J. Mol. Struct.* 1080 (2015) 162–168, <https://doi.org/10.1016/j.molstruc.2014.09.071>.
- R. Yerrasani, M. Karunakar, R. Dubey, A.K. Singh, R. Nandi, R.K. Singh, T.R. Rao, Synthesis, characterization and photophysical studies of rare earth metal complexes with a mesogenic Schiff-base, *J. Mol. Liq.* 216 (2016) 510–515, <https://doi.org/10.1016/j.molliq.2016.01.052>.
- N. Zhang, W. Peng, H. Guo, H. Wang, Y. Li, J. Liu, S. Zhang, P. Mei, T. Hayat, Y. Sun, Fabrication of porous carbon and application of Eu(III) removal from aqueous solutions, *J. Mol. Liq.* 280 (2019) 34–39, <https://doi.org/10.1016/j.molliq.2019.01.156>.
- K.R. Pellarin, R.J. Puddephatt, Oxidation of a dimethylplatinum(II) complex with oxaziridines: a hemiaminal intermediate but no oxo complex, *Organometallics* 32 (2013) 3604–3610, <https://doi.org/10.1021/om400079b>.
- Y. Zhou, D.S. Richeson, Bulky amidinate complexes of tin(IV). Synthesis and structure of Sn(RNC(R')NR')₂Cl₂ (R = cyclohexyl, R' = H, Me; R = SiMe₃, R' = t Bu), *Inorg. Chem.* 36 (1997) 501–504, <https://doi.org/10.1021/ic960940d>.
- W.J. Geary, The use of conductivity measurements in organic solvents for the characterisation of coordination compounds, *Coord. Chem. Rev.* 7 (1971) 81–122, [https://doi.org/10.1016/S0010-8545\(00\)80009-0](https://doi.org/10.1016/S0010-8545(00)80009-0).
- Z.A. Taha, A.M. Ajlouni, W. Al Momani, A.A. Al-Ghazawi, Syntheses, characterization, biological activities and photophysical properties of lanthanides complexes with a tetradentate Schiff base ligand, *Spectrochim. Acta - Part A Mol. Biomol. Spectrosc.* 81 (2011) 570–577, <https://doi.org/10.1016/j.saa.2011.06.052>.
- K. Binnemans, Y.G. Galyametdinov, R. Van Deun, D.W. Bruce, S.R. Collinson, A.P. Polishchuk, I. Bikhantaev, W. Haase, A.V. Prosvirin, L. Tinchurina, I. Litvinov, A. Gubajdullin, A. Rakhmatullin, K. Uytterhoeven, L. Van Meervelt, Rare-earth-

- containing magnetic liquid crystals, *J. Am. Chem. Soc.* 122 (2000) 4335–4344, <https://doi.org/10.1021/ja993351q>.
- [39] Z. Gao, Y. Wu, L. Xu, H. Hao, Q. Wu, H. Xie, Preparation and luminescent properties of Eu(III) organic complex and novel transparent ethylene-methyl acrylate copolymer (EMA) films doped with complexes, *Opt. Mater. (Amst)*. 85 (2018) 193–199, <https://doi.org/10.1016/j.optmat.2018.08.053>.
- [40] Y. Zhai, H. Xie, P. Cai, H.J. Seo, A luminescent inorganic-organic hybrid material containing the europium(III) complex with high thermal stability, *J. Lumin.* 157 (2015) 201–206, <https://doi.org/10.1016/j.jlumin.2014.08.059>.
- [41] F. Piccinelli, C. De Rosa, S. Zanzoni, M. Bettinelli, New Eu(III)-based complex with a C1 symmetric chiral ligand: a spectroscopic study, *J. Lumin.* 193 (2018) 114–118, <https://doi.org/10.1016/j.jlumin.2017.05.062>.
- [42] K. Binnemans, Interpretation of europium(III) spectra, *Coord. Chem. Rev.* 295 (2015) 1–45, <https://doi.org/10.1016/j.ccr.2015.02.015>.
- [43] J. Mei, J. Wang, J.Z. Sun, H. Zhao, W. Yuan, C. Deng, S. Chen, H.H.Y. Sung, P. Lu, A. Qin, H.S. Kwok, Y. Ma, I.D. Williams, B.Z. Tang, Siloles symmetrically substituted on their 2,5-positions with electron-accepting and donating moieties: facile synthesis, aggregation-enhanced emission, solvatochromism, and device application, *Chem. Sci.* 3 (2012) 549–558, <https://doi.org/10.1039/c1sc00688f>.
- [44] H. Li, Y. Guo, G. Li, H. Xiao, Y. Lei, X. Huang, J. Chen, H. Wu, J. Ding, Y. Cheng, Aggregation-induced fluorescence emission properties of dicyanomethylene-1,4-dihydropyridine derivatives, *J. Phys. Chem. C* 119 (2015) 6737–6748, <https://doi.org/10.1021/jp511060k>.
- [45] G. Han, D. Kim, Y. Park, J. Bouffard, Y. Kim, Excimers beyond pyrene: a far-red optical proximity reporter and its application to the label-free detection of DNA, *Angew. Chem. Int. Ed.* 54 (2015) 3912–3916, <https://doi.org/10.1002/anie.201410548>.
- [46] B. Ding, J. Zhang, W. Zhu, X. Zhen, Y. Wu, X.-Y. Jiang, et al., Fast and convenient determination of HOMO energy level of organic electroluminescent material using electrochemistry method, *Chem. Res. Appl.* 14 (6) (2002) 712–714.
- [47] D. Wang, X. Wang, Q. He, M. Zhou, W. Rui, X. Tao, F. Bai, M. Jiang, Enhanced two-photon absorption of novel four-branched chromophore via vibronic coupling, *Tetrahedron Lett.* 49 (2008) 5871–5876, <https://doi.org/10.1016/j.tetlet.2008.07.116>.
- [48] L. MacLean, D. Karcz, H. Jenkins, S. McClean, M. Devereux, O. Howe, M.D. Pereira, N.V. May, É.A. Enyedy, B.S. Creaven, Copper(II) complexes of coumarin-derived Schiff base ligands: pro- or antioxidant activity in MCF-7 cells? *J. Inorg. Biochem.* 197 (2019), 110702, <https://doi.org/10.1016/j.jinorgbio.2019.110702>.
- [49] Z.G. Wang, X.J. Ding, Y.Y. Huang, X.J. Yan, B. Ding, Q.Z. Li, C.Z. Xie, J.Y. Xu, The development of coumarin Schiff base system applied as highly selective fluorescent/colorimetric probes for Cu²⁺ and tumor biomarker glutathione detection, *Dyes Pigments* 175 (2020), 108156, <https://doi.org/10.1016/j.dyepig.2019.108156>.
- [50] G. He, X. Hua, N. Yang, L. Li, J. Xu, L. Yang, Q. Wang, L. Ji, Synthesis and application of a “turn on” fluorescent probe for glutathione based on a copper complex of coumarin hydrazide Schiff base derivative, *Bioorg. Chem.* 91 (2019), 103176, <https://doi.org/10.1016/j.bioorg.2019.103176>.
- [51] L. Yan, R. Li, W. Shen, Z. Qi, Multiple-color AIE coumarin-based Schiff bases and potential application in yellow OLEDs, *J. Lumin.* 194 (2018) 151–155, <https://doi.org/10.1016/j.jlumin.2017.10.032>.